

Structure and optical characterization of photochemically prepared ZrO₂ thin films doped with erbium and europium

G. Cabello^{a,*}, L. Lillo^a, C. Caro^a, G.E. Buono-Core^b, B. Chornik^c, M.A. Soto^d

^aDepartamento de Ciencias Básicas, Facultad de Ciencias, Universidad del Bío-Bío, Chillán, Chile

^bInstituto de Química, Pontificia Universidad Católica de Valparaíso, Valparaíso, Chile

^cDepartamento de Física, Facultad de Ciencias Físicas y Matemáticas, Universidad de Chile, Casilla 487-3, Santiago 8370415, Chile

^dDepartamento Química-Física, Facultad de Química, Pontificia Universidad Católica de Chile, Casilla 306, Santiago 609441, Chile

A B S T R A C T

Zirconium oxide thin films loaded with 10, 30 and 50 mol% lanthanide ions (Er or Eu) have been successfully prepared by direct UV (254 nm) irradiation of amorphous films of β -diketonate complexes on Si(100) substrates, followed by a post annealing treatment process. The resultant films were characterized by X-ray photoelectron spectroscopy and Atomic Force Microscopy. The results showed that the stoichiometry of the resulting films were in relative agreement with the composition of the precursor films. The effects of annealing as well as the lanthanide ion loading on the photoluminescence (PL) emission intensity were investigated, finding that thermal treatment decreases surface roughness as well as PL emission intensity.

Keywords:

Spin coating

Luminescence

XPS

Photo-deposition

1. Introduction

Photoluminescence properties of many metal oxides such as TiO₂ [1], ZnO [2], WO₃ [3] and In₂O₃ [4] have attracted considerable interest, because they may be used in many fields, such as nanoscopic optical storage elements, or as probes in living systems [5]. However, comparatively few studies have been carried out concerning the photoluminescence (PL) of ZrO₂, especially rare earth doped ZrO₂, such as ZrO₂-Er [6,7], ZrO₂-Eu [8,9] and ZrO₂-Sm [10,11] systems.

However, for developing effective luminescence devices, materials with much lower phonon energy should be selected as hosts because the high phonon energy of the host lattice is responsible for non-radiative relaxation. SiO₂ matrix (phonon energy: 1100 cm⁻¹) is widely used as a host due to their high transparency in the visible region. However, the network structure of SiO₂ makes it impossible to introduce high content of dopant without clustering which leads to concentration quenching of emission [12].

ZrO₂ is one of the candidates for the substitution of SiO₂ as host matrix for lanthanide ion due to its chemical and photochemical

stability, high refractive index and low phonon energy. The stretching mode of the ZrO₂ is about 470 cm⁻¹ which is much lower than that for Al₂O₃ (870 cm⁻¹) or SiO₂ (1100 cm⁻¹) [12].

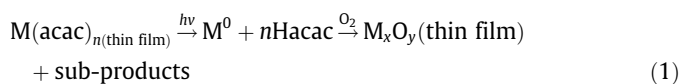
Various metal ions incorporated into Zirconia materials can achieve special optical properties. Placing f-electron elements in Zirconia-based materials has the potential for solid-state photonic device applications. The ability to stabilize each crystalline phase of Zirconia at ambient temperature provides an opportunity for correlating the optical properties with the structure. In addition, structural modifications may impact the electronic structure of the lattice, and useful chemical and optical properties could emerge. As the main structural difference between these Zirconia phases is due to displacements of the oxygen atoms in the lattice, it is of interest to follow the spectroscopic consequences which accompany the structural modifications [10].

Several preparation techniques have been proposed to fabricate ZrO₂ thin films by dry processes, such as sputtering [13], chemical vapor deposition (CVD) [14] and atomic layer deposition (ALD) [15] and by moist processes such as sol-gel [16] and liquid phase deposition (LPD) [12]. Among these methods, the photochemical deposition technique is a promising and powerful method for fabricating loaded and unloaded ZrO₂ thin films due to its simplicity and low energy consumption.

* Corresponding author. Tel.: +56 42 253096; fax: +56 42 253046.

E-mail address: gcabello@ubiobio.cl (G. Cabello).

In previous articles we have reported a photochemical method for the deposition of a variety of metals and metal oxides [17–19]. In this method, also known as PMOD (photochemical metal organic deposition), thin films of inorganic or organometallic precursors are converted upon irradiation to amorphous films of metals or oxides, depending on the reactions conditions. The development of this method requires that the precursor complexes form stable amorphous thin films upon spin coating onto a suitable substrate and the photolysis of these films results in the photoextrusion of the ligands leaving the inorganic products on the surface as shown in Eq. (1).



where: M = Zr, Eu or Er; acac = acetylacetonate ligand.

In the present work, we report the preliminary results on the characterization of zirconium oxide thin films loaded with lanthanide elements (Er³⁺ or Eu³⁺) prepared by photochemical deposition.

2. Experimental

2.1. General procedure

Fourier Transform Infrared spectra (FT-IR) were obtained with 4 cm⁻¹ resolution in a Perkin Elmer Model 1605 FT-IR spectrophotometer.

UV spectra were obtained with 1 nm resolution in a Perkin Elmer Model Lambda 25 UV-Vis spectrophotometer.

X-ray photoelectron spectra (XPS) were recorded on an XPS-Auger Perkin Elmer electron spectrometer Model PHI 1257 which included an ultra high vacuum chamber, a hemispherical electron energy analyzer and an X-ray source providing unfiltered K α radiation from its Al anode ($h\nu = 1486.6$ eV). The pressure of the main spectrometer chamber during data acquisition was maintained at ca 10⁻⁷ Pa. The binding energy (BE) scale was calibrated by using the peak of adventitious carbon, setting it to 284.6 eV. The accuracy of the BE scale was ± 0.1 eV. High resolution spectra were always fitted using Gaussian-Lorentzian curves in order to more accurately determine the BE of the different element core levels. Prior to curve fitting, a background was subtracted by the method devised by Shirley [20]. The approximate composition of the surface was determined by dividing the individual peak area, after appropriate background subtraction, by their respective atomic sensitivity factor (ASF).

X-ray diffraction patterns were obtained using a D5000 X-ray diffractometer. The X-ray source was CuK α ($\lambda = 1.5405$ Å) and measurements were taken in the 2θ range 0–90°.

Atomic Force Microscopy (AFM) was performed in a Nanoscope IIIa (Digital Instruments, Santa Barbara, CA) in contact mode. Film thickness was determined using a Leica DMLB optical microscope with a Michelson interference attachment.

The solid state photolysis was carried out at room temperature under a low-pressure Hg lamp ($\lambda = 254$ nm) equipped with two 6 W tubes, in an air atmosphere. Progress of the reactions was monitored by determining the FT-IR spectra at different time intervals, following the decrease in IR absorption of the complexes.

The substrates for deposition of films were Indium Tin oxide (ITO) covered glass (1 × 2 cm) and n-type silicon(100) wafers (1 × 1 cm) obtained from Wafer World Inc, Florida.

Fluorescence emission spectra measurements were carry out in a multifrequency phase fluorometer (K2, ISS Inc., Urbana, Campaign, IL, USA) with a L type setup. Excitation was performed with a 400 W UV Xe arc lamp. Excitation monochromator was set at 465 nm for ZrO₂-Eu films and at 488 nm for ZrO₂-Er films, were taken at room temperature.

2.2. Preparation of amorphous thin films

The precursors Zr(IV) acetylacetonate, and lanthanides complexes Er(III) and Eu(III) acetylacetonate were purchased from Aldrich Chemical Company and thin films were prepared by the following procedure: A silicon chip was placed on a spin coater and rotated at a speed of 1500 RPM. A portion (0.1 ml) of a solution of the precursor complex in CH₂Cl₂ was dispensed onto the silicon chip and allowed to spread. The motor was stopped after 30 s and a thin film of the complex remained on the chip. The quality of the films was examined by optical microscopy (1000× magnification).

2.3. Photolysis of complexes as films on Si(100) surfaces

All photolysis experiments were done following the same procedure. Here is the description of a typical experiment. A film of the complex was deposited on n-type Si(100) by spin-coating from a CH₂Cl₂ solution. This resulted in the formation of a smooth, uniform coating on the chip. The quality of the precursor films (uniformity, defects, etc.) was determined by optical microscopy (1000×), while the thickness was monitored by interferometry. The FT-IR spectrum of the starting film was first obtained. The irradiation of the films was carried out at room temperature in air atmosphere, until the FT-IR spectrum showed no evidence of the starting material. Prior to analysis the chip was rinsed several times with dry acetone to remove any organic products remaining on the surface. In order to obtain films of a specific thickness, successive layers of the precursors were deposited by spin-coating and irradiated as above. This process was repeated several times until the desired thickness was achieved.

Normally, the deposition of five successive layers were needed to obtain films of 300–450 nm thickness. Post-annealing was carried out under a continuous flow of synthetic air at 500 °C for 2 h. in a programmable Lindberg tube furnace.

3. Results and discussion

In a previous paper we reported that films of the Zr(acac)₄ complex deposited on Si(100) by spin-coating and irradiated under air atmosphere with a 254 nm UV source gives rise to thin films of ZrO₂ [21]. In order to evaluate the photoreactivity of the Er and Eu complexes, thin films of the acetylacetonate complexes were irradiated and the photolysis monitored by FT-IR spectroscopy. It was observed that the band at 1518 cm⁻¹ (associated with the carbonyl group of the ligand) decreases in intensity, and after 36 h of irradiation only a minimal absorption remains. These results suggest that the diketonate groups on the precursor material are photodissociated on the surface, forming volatile products which are partially desorbed.

3.1. Characterization of ZrO₂-Ln photodeposited thin films (where Ln = Er or Eu)

For the deposition of ZrO₂-Ln thin films, solutions of Zr(acac)₄ with different proportions of the Ln(acac)₃ complexes (10, 30 and 50 mol%) were spin-coated on the appropriate substrate and the films irradiated until no IR absorptions due to the precursors were observed.

3.1.1. XPS and XRD analysis

Chemical compositions of the ZrO₂-Ln thin films, both as-deposited and annealed at 500 °C were characterized by XPS (see Fig. 1 and 2). For the as-deposited thin films, spectra show that O, Zr and C were present. The C1s peak appearing near 284.9 eV

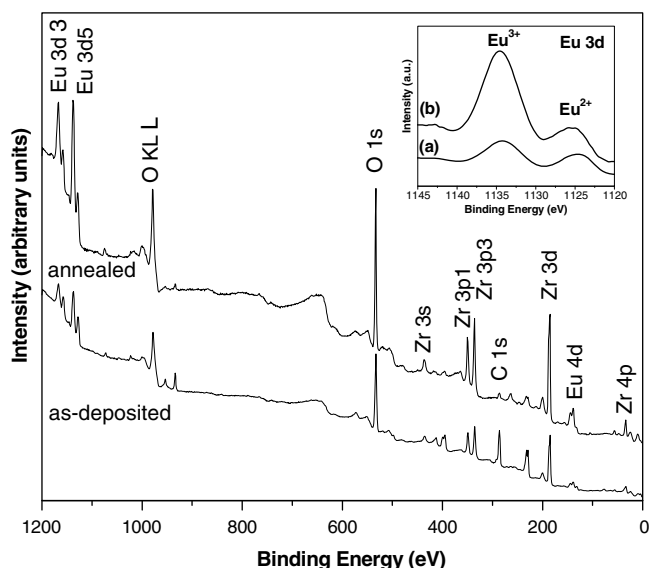


Fig. 1. XPS survey spectrum of an as-deposited and annealed at 500 °C ZrO_2 -Eu thin films prepared by UV irradiation at 254 nm. Inset figure: Eu 3d core level XPS spectra of ZrO_2 -Eu thin films: (a) as-deposited, and (b) annealed thin films.

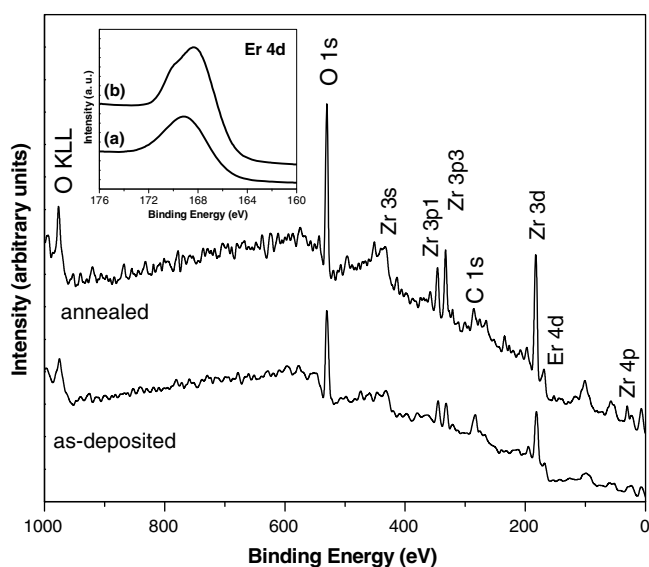


Fig. 2. XPS survey spectrum of an as-deposited and annealed at 500 °C ZrO_2 -Er thin films prepared by UV irradiation at 254 nm. Inset figure: Er 4d core level XPS spectra of ZrO_2 -Er thin films: (a) as-deposited, and (b) annealed thin films.

can be attributed to the organic residual from the precursor. It was also detected after annealing at 500 °C, although its intensity

became significantly lower. Peaks from other impurities such as N and Si (attributed to the substrate) were not detected.

Other authors have reported that metal β -diketonates such as $[Zr(acac)_4]$ require higher substrate temperatures (>600 °C) for oxide growth, and can lead to carbon incorporation in metal-organic chemical vapor deposition (MOCVD) [22,23].

Our measured binding energy values of the Zr $3d_{5/2}$, O 1s and Ln (where Ln = Eu or Er) for the as-deposited and annealed films are shown in Table 1.

XPS spectra showed that the Zr 3d range for the as-deposited film was composed of two peaks with binding energies of 182.0 eV ($3d_{5/2}$ level) and 184.4 eV ($3d_{3/2}$ level) (Fig. 3(a)). The observed binding energy for Zr $3d_{5/2}$ is higher than those reported for Zr metal (180.0 eV) and ZrO_x (181.4 eV for $0 < x < 2$), but close to 182.0 eV for ZrO_2 [24]. After annealing at 500 °C, the binding energies were 182.2 and 184.6 eV for Zr $3d_{5/2}$ and Zr $3d_{3/2}$ levels, respectively.

The O 1s peak can be fitted with two peaks located 530.0 and 532.1 eV (Fig. 3(b)). The first peak located at a lower energy is attributed to Zr-O bonds [25], while the second one, located at higher energy, corresponds to O-H bonds from absorbed water molecules [24]. This peak weakened significantly after annealing at 500 °C.

The quantitative analysis was calculated from the normalized areas of the Zr 3d and the O 1s peaks, using the atomic sensitivity factors. It shows a molar ratio of Zr/O = 1:1.2 for the as-deposited thin film, which is much smaller than the value for stoichiometric ZrO_2 , suggesting that oxygen is partially bound as OH or H_2O . However a stoichiometric composition of Zr/O = 1:2 was obtained on the annealed sample, but the small peak for Zr-OH in the Zr 3d range confirmed that the elimination of impurities (mostly in the form of H_2O or OH) was not complete even after annealing at 500 °C.

For ZrO_2 -Eu thin films the Eu $3d_{5/2}$ signal shows two well resolved peaks centered at 1134.2 and 1125.0 eV binding energy (Inset Fig. 1). Similar values has been reported for other authors [26–28]. The higher binding energy peak is related to the (3+) oxidation state and the lower binding energy peak corresponds to a (2+) oxidation state, in accordance with Ramos et al. [26]. The relative contribution of these two components to the spectrum, as determined by fitting, is respectively, 56% (Eu^{3+}) and 42% (Eu^{2+}) for the as-deposited sample. After annealing at 500 °C the relative contributions of Eu^{3+} and Eu^{2+} states are drastically modified, becoming 75% and 25%, respectively. This change in the relative contribution can be understood by the fact that annealing leads to partial oxidation of Eu^{2+} to Eu^{3+} .

On the other hand, for the ZrO_2 -Er thin films, the broad peak in the Er $4d_{5/2}$ (Inset Fig. 2) centered at a B.E. of 169.2 and 168.3 eV for as-deposited and annealed thin films, respectively, corresponds to Er_2O_3 or Er(III) species. Similar values have been reported by other authors [29–32].

Table 1

XPS results (binding energies, eV) for the ZrO_2 -Ln thin films; the values between parentheses indicate the relative percentages of peak areas

Thin films	Zr $3d_{5/2}$	O 1s	Eu $3d_{5/2}$	Er $4d_{5/2}$
ZrO_x -Eu ^a	182.0 ± 0.1	529.9 ± 0.1 (81.1) 532.1 ± 0.1 (19.9)	1134.3 ± 0.1 (56.2) 1125.0 ± 0.1 (42.4)	
ZrO_2 -Eu ^b	182.3 ± 0.1	530.1 ± 0.1 (88.7) 531.9 ± 0.1 (11.3)	1134.2 ± 0.1 (74.6) 1125.6 ± 0.1 (25.4)	
ZrO_x -Er ^a	182.0 ± 0.1	530.1 ± 0.1 (57.9) 531.2 ± 0.1 (42.1)		169.2 ± 0.1 (89.1)
ZrO_2 -Er ^b	182.4 ± 0.1	530.0 ± 0.1 (53.3) 531.4 ± 0.1 (46.7)		168.3 ± 0.1 (92.0)

^a As-deposited.

^b Annealed at 500 °C for 2 h.

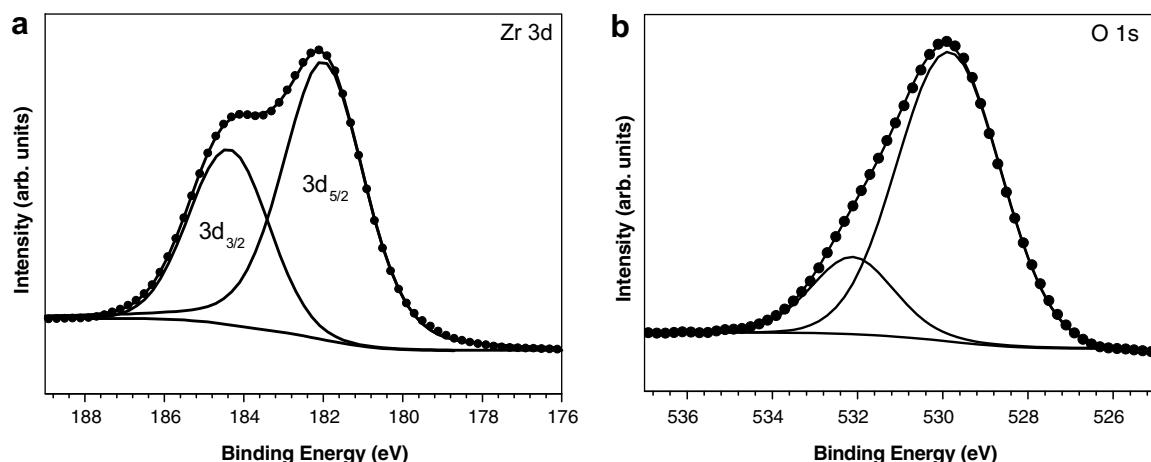


Fig. 3. Curve fitting results of: (a) Zr 3d band spectra, and (b) O 1s band spectra of ZrO_2 -Ln thin films.

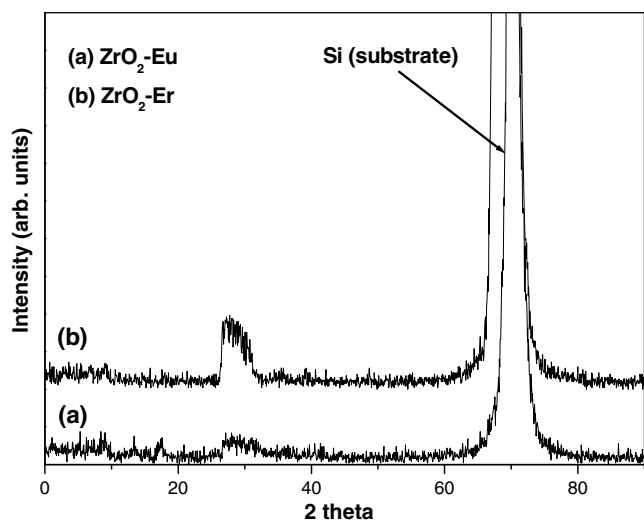


Fig. 4. XRD spectra of (a) ZrO_2 -50%-Eu, and (b) ZrO_2 -50%-Er thin films annealed at 500 °C.

Table 2
AFM results for the ZrO_2 -Ln thin films

Thin films	Rms (nm)	
	10%-Ln	50%-Ln
ZrO_x -Eu ^a	6.90 (65.3)	28.5 (228)
ZrO_2 -Eu ^b	3.18 (27.5)	19.6 (116)
ZrO_x -Er ^a	83.9 (416)	11.2 (133)
ZrO_2 -Er ^b	5.54 (43.3)	1.42 (24.0)

Values in parenthesis show the R_{max} maximum height (nm).

^a As-deposited.

^b Post-annealed at 500 °C for 2 h.

The X-ray diffraction analysis of ZrO_2 -Ln films prepared on Si(100) substrates is shown in Fig 4. After annealing at 500 °C, only peaks corresponding to Si(100) at angles of 33.0° and 69.1° can be observed which confirmed the amorphous nature of the films.

3.1.2. Film morphology

AFM was used to study the morphology of the photodeposited films and the results are summarized in Table 2.

Fig. 5 shows the AFM micrographs corresponding to ZrO_2 -Eu films loaded with 10, 30 and 50 mol% of Eu respectively. The as-

deposited films has a non-uniform rough surface, with rms values increasing with the amount of europium present in the films. This can be explained by the presence of two species of europium, Eu^{+2} and Eu^{+3} (as shown by XPS analysis, Fig. 1). After these films were annealed at 500 °C, rms values decrease significantly, and a more regular and uniform film surface can be observed. We attribute this reduction in roughness to the fact that great part of the byproducts generated during photolysis are eliminated from the surface of the films as a result of thermal treatment. This in turn produces a redistribution of the deposits on the surface generating a more compact and uniform film.

On the other hand, the as-deposited ZrO_2 -Er thin films (Fig. 6) present a non-uniform rough surface topography, with rms values decreasing as the amount of erbium present in the films increases, as shown in Table 2.

The different surface roughness of the ZrO_2 -Er as-deposited films loaded with 10, 30 and 50 mol% of Er may be explained by the formation of a smoother Er_2O_3 film surface.

The surface morphology of these deposits also varied remarkably after annealing at 500 °C. Very smooth and homogeneous surfaces formed by nanometer-sized small grains are obtained, especially for ZrO_2 loaded with 50 mol% of Er, which consisted of grains with sizes between 50 and 120 nm. The grain size and its distribution play an important role on the densification processes. Small grains and a narrow size distribution probably help in obtaining a dense and homogeneous film. Some authors have reported that annealing can suppress the formation of Er silicate (Si substrate) at the interface during film growth, thus favoring the formation of Er_2O_3 films with smooth surfaces [33]. XPS analysis (Fig. 2) confirmed the presence of Er^{+3} in the films.

3.1.3. Transparency and optical band gap

For determination of optical properties, the ZrO_2 -Ln thin films were prepared on ITO covered glass substrates under the same conditions as those prepared on Si substrates. High optical transmission in the visible region is required for luminescence materials to obtain the effective emission [12]. Optical transmission for as grown films was measured in the range 300–900 nm using a spectrophotometer. These transmission spectra are shown in Fig. 7.

The as-deposited and annealed samples both showed little absorption in the visible region, implying high transparency. In fact, the mean transmittance in the visible region was over 60% and 80% for the as-deposited and annealed ZrO_2 -Ln thin films, respectively, on the basis of transmittance spectra (Fig. 7). The high

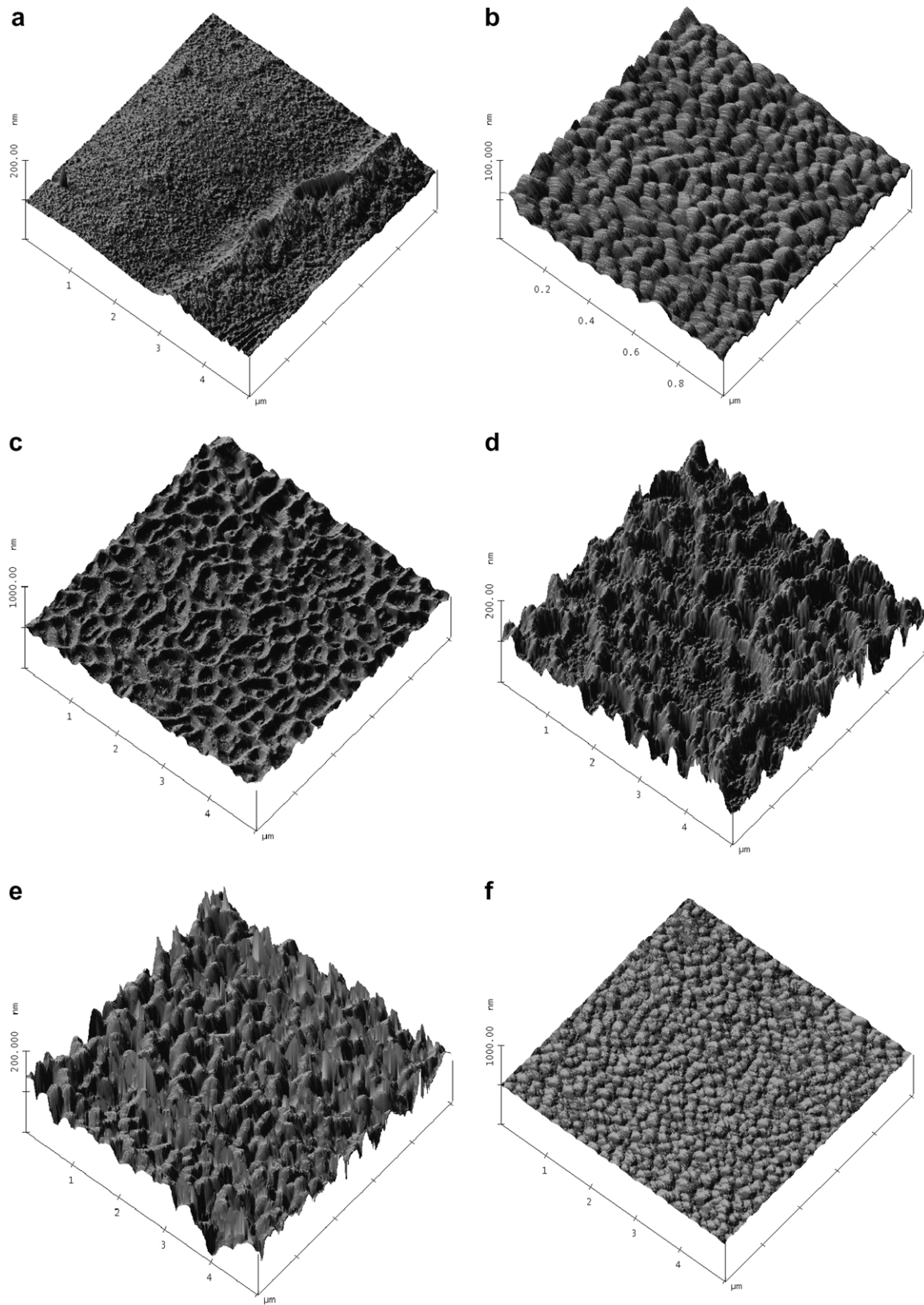


Fig. 5. AFM images ($5 \times 5 \mu\text{m}$) of europium loaded zirconium oxide films with: (a) as-deposited 10% Eu, (b) annealed 10% Eu ($1 \times 1 \mu\text{m}$), (c) as-deposited 30% Eu, (d) annealed 30% Eu, (e) as-deposited 50% Eu, and (f) annealed 50% Eu.

transparency of the annealed $\text{ZrO}_2\text{-Ln}$ thin films indicates fairly smooth surfaces and relatively good film homogeneity formed by

nanometer-sized small grains, and evidently due to the low surface roughness, which is consistent with the AFM observations.

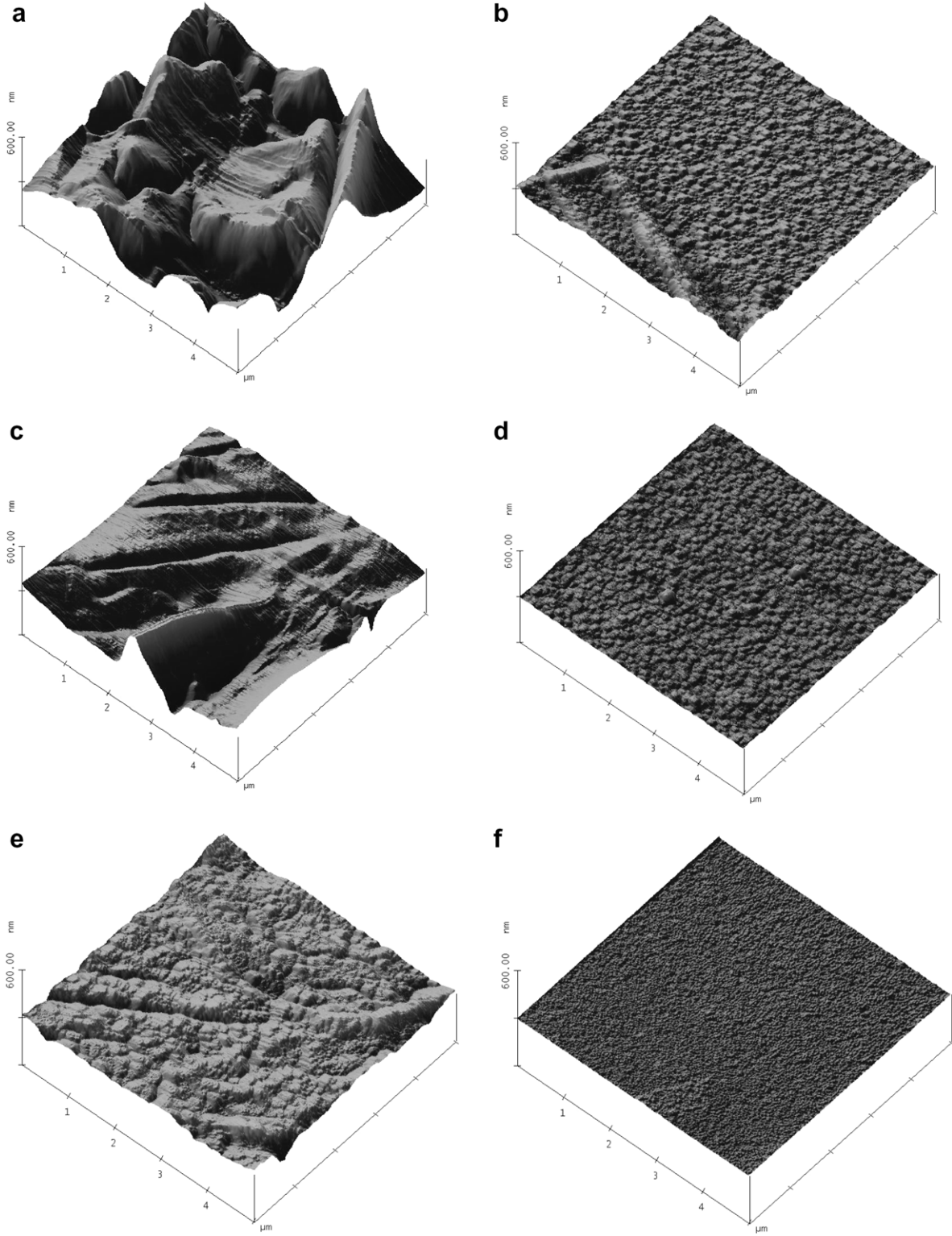


Fig. 6. AFM images ($5 \times 5 \mu\text{m}$) of erbium loaded zirconium oxide films with: (a) as-deposited 10% Er, (b) annealed 10% Er, (c) as-deposited 30% Er, (d) annealed 30% Er, (e) as-deposited 50% Er, and (f) annealed 50% Er.

The optical absorption coefficient, α , which is the relative rate of decrease in light intensity along its propagation path, was calculated from the transmittance (T) data in the wavelength range 300–900 nm. The nature of the optically induced transitions was determined from these data [24,34]. The optical absorption coefficient of films was evaluated using the relation

$$\alpha = -\ln(T)/d \quad (2)$$

where d is the film thickness.

It is well known that the fundamental absorption refers to the transition from the valence band (VB) to the conduction band (CB) from which the band gap energy (E_g) can be estimated assuming a direct transition between the bands [34,35]. The $(\alpha h\nu)^2$ vs.

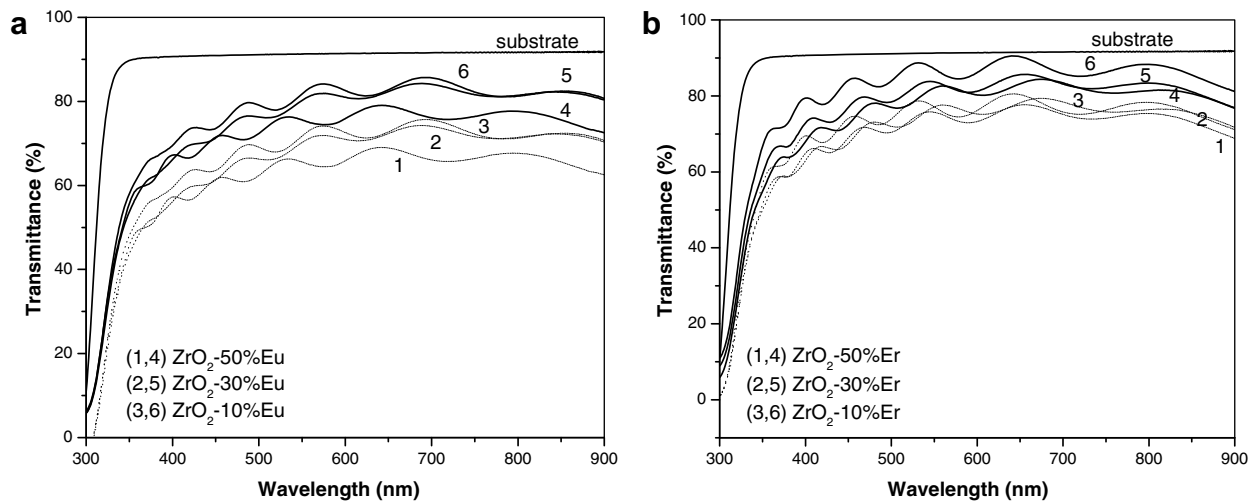


Fig. 7. Transmission spectra of (—) as-deposited and (---) annealed (at 500 °C): (a) ZrO₂-Eu, and (b) ZrO₂-Er thin films grown on ITO covered glass substrates.

photon energy ($h\nu$) is derived from the optical transmission spectra of the ZrO₂-Ln thin films measured by UVS, where α is absorption coefficient. The absorption coefficient α as a function of photon energy $h\nu$ can be expressed as

$$(\alpha h\nu)^2 = C(h\nu - E_g) \quad (3)$$

where C is a constant. Therefore, the band-gap energy of the thin films can be obtained by extrapolating the linear portion of the curves relating $(\alpha h\nu)^2$ vs. $h\nu$ to $(\alpha h\nu)^2 = 0$.

Using the function $(\alpha h\nu)^{1/2}$ for an indirect transition did not show a linear character which indicates that our samples have a direct band-gap.

The values of band-gap energy for unloaded as-deposited and annealed ZrO₂ films were determined to be 5.5 and 5.8 eV, respectively, [21]. These values are too large to absorb and utilize visible light [36]. It has been reported that incorporation of metal ions into the ZrO₂ thin films resulted in red-shifts in the absorption spectra. This observation suggests that impurity levels are introduced between the intrinsic bands which subsequently generate new band gaps [37]. The effects that dopants have on the performance of ZrO₂ are mainly associated with modifying the microstructure as well as reducing the band gaps [37].

Ln-loaded ZrO₂ thin films showed lower band gap values than unloaded films. The band gap energies for as-deposited and annealed ZrO₂-Eu thin films were calculated to be about 4.20–4.25 eV and 4.10–4.17 eV, respectively.

On the other hand, the band gap energy values determined for the as-deposited and annealed ZrO₂-Er thin films were 4.21–4.28 eV and 4.12–4.18 eV, respectively. We attribute the slight decrease in band gap energies after annealing of the ZrO₂-Ln films to the oxidation states of metal ions. The differences in band gaps are mainly associated with the electronic configurations of the ions, which control the energy levels in ZrO₂. The partial oxidation of lanthanide ion Ln²⁺ to Ln³⁺ after annealing (from our XPS results), help to support this conclusion. Similar phenomena were also observed in previous studies but with other metals-doped [37,38].

3.2. Photoluminescence study of the ZrO₂-Ln thin films

The photoluminescence (PL) experiment of the ZrO₂-Eu thin films was performed in the range of 650–750 nm at an excitation wavelength of 465 nm at room temperature. Similar values of excitation have been used in other works [39]. This wavelength corresponds to a strong ⁷F₀ → ⁵D₂ absorption transition of the Eu³⁺ ion [40]. The excitation spectra of as-deposited and annealed

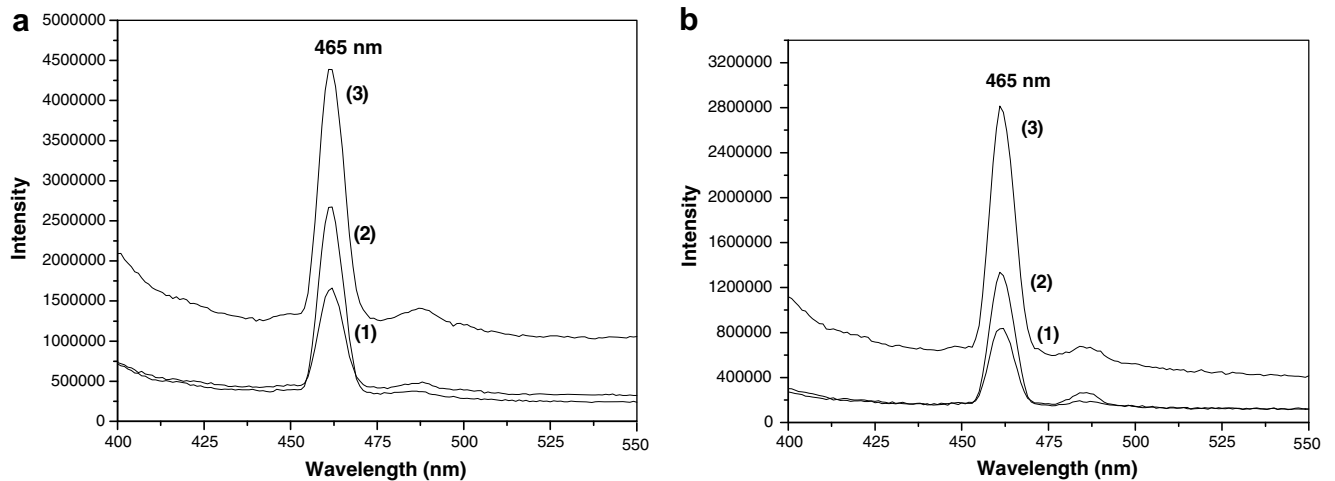


Fig. 8. Excitation spectra of (a) as-deposited, and (b) annealed at 500 °C ZrO₂-Eu thin films: (1) 10% Eu, (2) 30% Eu, and (3) 50% Eu.

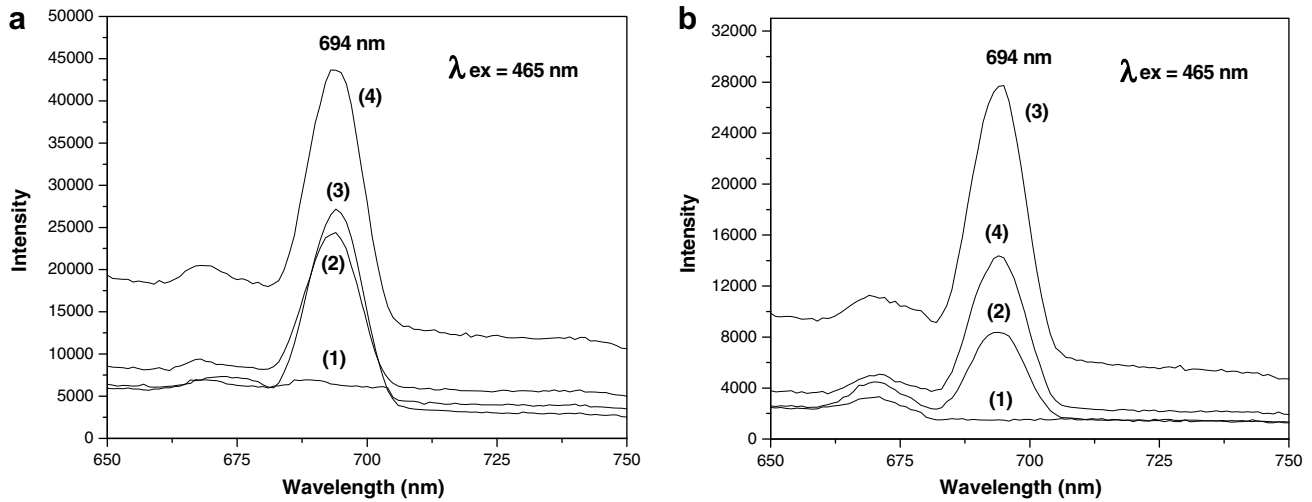


Fig. 9. The PL spectrum of (a) as-deposited, and (b) annealed at 500 °C ZrO_2 -Eu thin films excited at 465 nm: (1) unloaded ZrO_2 , (2) 10% Eu, (3) 30% Eu, and (4) 50% Eu.

Eu^{3+} loaded ZrO_2 films are shown in Fig 8. In both cases the excitation spectra consist of a broad band which increased intensity as the amount of Eu loaded on ZrO_2 host also increases. This could be attributed to the possibility of energy transfer from the host (donor) to the loaded ion (acceptor) and to the increase interaction between Eu^{3+} ions present and the oxygen available in the matrix.

Photoluminescence (PL) spectra of the ZrO_2 -Eu thin films excited at 465 nm are shown in Fig 9. The spectra are composed of a large broad band in the red spectral region corresponding to a ${}^5D_0 \rightarrow {}^7F_4$ transition. As seen in Fig 9(a), for as-deposited ZrO_2 -Eu films, the intensity of this emission band increases with loaded of Eu^{3+} on the ZrO_2 matrix, as expected. However, for the annealed ZrO_2 -Eu films, Fig 9(b), it can be seen that although the Eu^{3+} emission intensities also increase with concentration, it reaches a maximum value at 30 mol% Eu^{3+} loaded, and decreases rapidly with further increase in the Eu^{3+} concentration, probably due to concentration quenching (self-quenching).

It has been reported by Chen et al. [8] that the different luminescence properties of metal oxides depend on different bond lengths between the dopant metal and the oxygen in the matrix.

The charge transfer state (CT) band of Eu^{3+} in oxides has been studied and concluded that the CT position of an Eu^{3+} doped oxide depends on the Eu-O length and on the coordination environment around Eu^{3+} . With increasing bond length, the band shifts to lower energies and the luminescence intensity is also related the Eu-O bond distance, so that the shorter the bond length, the higher the luminescence intensity [41]. However, given the amorphous nature of our thin films, the emission intensities increase with ion loading, but the films may remain amorphous after annealing which could affect the emission intensities.

Photoluminescence excitation spectra of as-deposited and annealed ZrO_2 -Er thin films are shown in Fig. 10. It can be seen that the PL spectra mainly consist of two intense bands between 450 and 500 nm, and a small band located at 405–407 nm. These absorption bands, centered at 471 and 488 nm for the as-deposited films (Fig. 10(a)), and 463 and 488 nm for the annealed films (Fig. 10(b)), could be attributed to energy-transfer mechanisms between the host matrix and the Er^{3+} ions. In other words, the interaction between host lattice oxygen atoms and Er^{3+} is determinant.

Photoluminescence for the ZrO_2 -Er thin films was obtained at a excitation wavelength of 488 nm, similar to values used in other

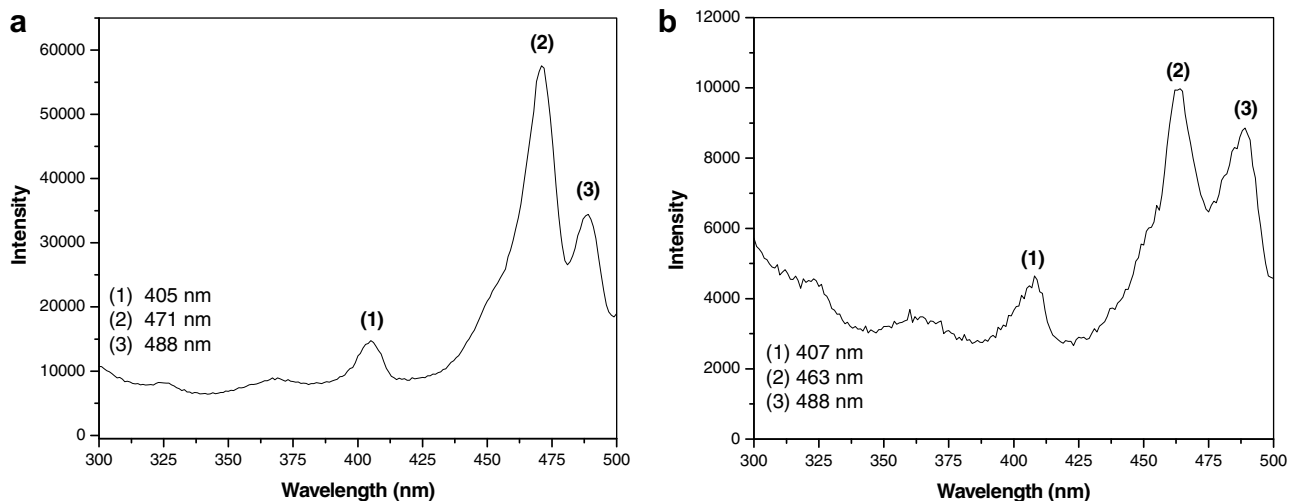


Fig. 10. Excitation spectra of (a) as-deposited, and (b) annealed at 500 °C ZrO_2 -50%-Er thin films.

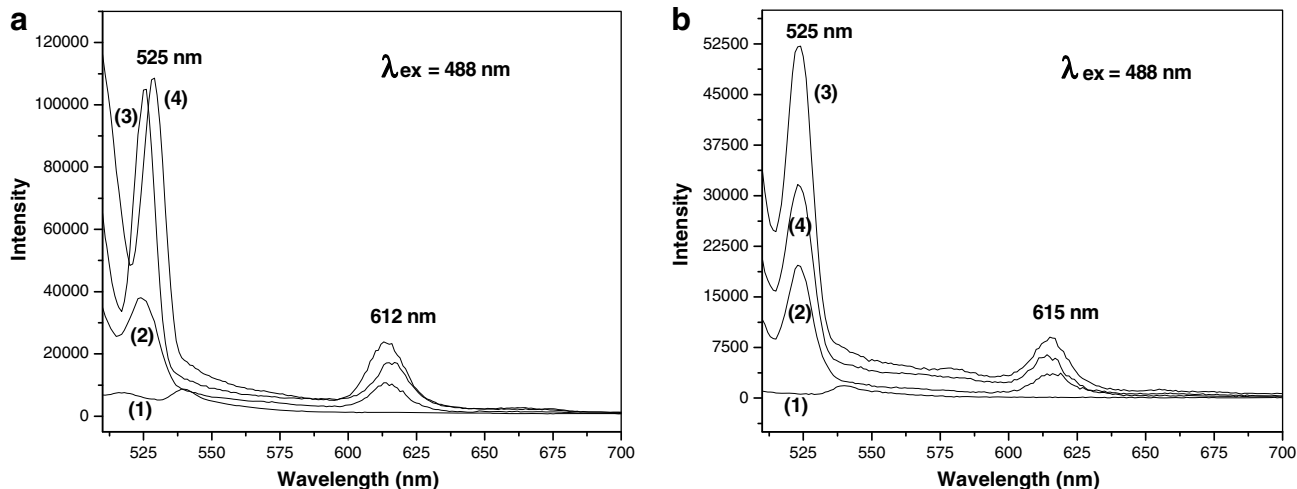


Fig. 11. The PL spectrum of (a) as-deposited, and (b) annealed at 500 °C ZrO_2 -Er thin films excited at 488 nm: (1) unloaded ZrO_2 , (2) 10% Er, (3) 30% Er, and (4) 50% Er.

studies [6,7,42]. Fig 11 shows the characteristic PL emission spectra determined between 500 nm and 700 nm at room temperature. An emission spectral peak centered at 525 nm (green) can be seen, corresponding to ${}^2H_{11/2} \rightarrow {}^4I_{15/2}$ transition [6,7,43], and another smaller peak at 612–615 nm (orange–red) is observed, probably attributed to stark splitting of the degenerate 4f levels under the crystalline field and the amorphous nature of the films, in the surroundings of the erbium ions. These new bands appear as a consequence of changes in the Er^{3+} ions site from the force of the crystal field on f–f transitions.

It can be observed from Fig. 11(a) (as-deposited films), that as the Er concentration increases, the emission centered at 525 nm becomes dominant, reaching a maximum intensity at 30 and 50 mol% Er loading. However, after annealing, the sample containing 30 mol% of Er presents the greater intensity, while the sample with 50 mol% Er loading shows a much lower intensity (Fig. 11(b)). A possible explanation for this effect is the surface reorganization of the annealed films which at higher loading (50 mol%) may cause the formation of some clusters of Er^{3+} ions which may result in concentration quenching of Er^{3+} luminescence.

4. Conclusion

In summary, Eu and Er loaded ZrO_2 amorphous thin films were prepared by a photodeposition method at room temperature from β -diketonate complexes. XPS results showed that the composition of the resulting films is what we would expect from the employed precursors. The amorphous characteristic of the precursor complexes strongly determine the non-crystalline nature of the as-deposited metal oxide films and its optical and photoluminescent properties. However, post-thermal treatment of the photodeposited films favors stoichiometric, surface homogeneity, and transparency. A more detailed study is required to determine the photoluminescent properties of the obtained films.

Acknowledgements

The authors are grateful for the financial support of FONDECYT (Fondo Nacional de Desarrollo Científico y Tecnológico), Chile. Grant No. 1060486, Dirección de Investigación de la U. del Bío-Bío, DIUBB proyect. Grant No. 073909 2/R and Dirección de Investigación y Postgrado, Pontificia Universidad Católica de Valparaíso (DI 125.717/07).

References

- [1] Z. Liu, J. Zhang, B. Han, J. Du, T. Mu, Y. Wang, Z. Sun, *Micropor. Mesopor. Mater.* 81 (2005) 169.
- [2] P. Che, J. Meng, L. Guo, *J. Lumin.* 122&123 (2007) 168.
- [3] J.H. Hao, J. Gao, *Appl. Surf. Sci.* 252 (2006) 5590.
- [4] M-SM.-S. Lee, W. Choi, E. Kim, C. Kim, S-K.S.-K. Min, *Thin Solid Films* 279 (1996) 1.
- [5] L.-J. Lai, H.-C. Lu, H.-K. Chen, B.-M. Cheng, M.-I. Lin, T.-C. Chu, *J. Electron Spectrosc.* 144–147 (2005) 865.
- [6] N. Maeda, N. Wada, H. Onoda, A. Maegawa, K. Kojima, *Thin Solid Films* 445 (2003) 382.
- [7] R. Jia, W. Yang, Y. Bai, T. Li, *Opt. Mater.* 28 (2006) 246.
- [8] L. Chen, Y. Liu, Y. Li, *J. Alloys Compd.* 381 (2004) 266.
- [9] Z.W. Qian, L.S. Wang, J. Lin, *Mater. Res. Bull.* 40 (2005) 810.
- [10] Z. Assefa, R.G. Haire, P.E. Raison, *Spectrochim. Acta A* 60 (2004) 89.
- [11] V. Kiisk, I. Sildos, S. Lange, V. Reedo, T. Tatte, M. Kirm, J. Aarik, *Appl. Surf. Sci.* 247 (2005) 412.
- [12] K. Kuratani, M. Mizuhata, A. Kajinami, S. Deki, *J. Alloys Compd.* 408–412 (2006) 711.
- [13] L.D. Huy, P. Laffez, Ph. Daniel, A. Jouanneaux, N.T. Khoi, D. Simeone, *Mater. Sci. Eng. B* 104 (2003) 163.
- [14] R. Thomas, A. Milanov, R. Bhakta, U. Patil, M. Winter, P. Ehrhart, R. Waser, A. Devi, *Chem. Vap. Deposition* 12 (2006) 295.
- [15] D.M. Hausmann, R.G. Gordon, *J. Cryst. Growth* 249 (2003) 251.
- [16] E. De la Rosa-Cruz, L.A. Diaz-Torres, P. Salas, D. Mendoza, J.M. Hernandez, V.M. Castaño, *Opt. Mater.* 19 (2002) 195.
- [17] G.E. Buono-Core, G. Cabello, B. Torrejon, M. Tejos, R.H. Hill, *Mater. Res. Bull.* 40 (2005) 1765.
- [18] G.E. Buono-Core, M. Tejos, G. Cabello, N. Guzmán, R.H. Hill, *Mater. Chem. Phys.* 96 (2006) 98.
- [19] G.E. Buono-Core, G.A. Cabello, H. Espinoza, A.H. Klahn, M. Tejos, R.H. Hill, *J. Chin. Chem. Soc.* 51 (2006) 950.
- [20] D. Shirley, *Phys. Rev. B* 5 (1972) 4709.
- [21] G. Cabello, L. Lillo, G.E. Buono-Core, *J. Non-Cryst. Solids* 354 (2008) 982.
- [22] P.A. Williams, J.L. Roberts, A.C. Jones, P.R. Chalker, J.F. Bickley, A. Steiner, H.O. Davies, T.J. Leedham, *J. Mater. Chem.* 12 (2002) 165.
- [23] Y.F. Loo, R. Okane, A.C. Jones, H.C. Aspinall, R.J. Potter, P.R. Chalker, J.F. Bickley, S. Taylor, L.M. Smith, *J. Mater. Chem.* 15 (2005) 1896.
- [24] Y. Gao, Y. Masuda, H. Ohta, K. Koumoto, *Chem. Mater.* 16 (2004) 2615.
- [25] J.C. Dupin, D. Gonbeau, P. Vinatier, A. Levasseur, *Phys. Chem. Chem. Phys.* 2 (2000) 1319.
- [26] S.M.M. Ramos, B. Canut, P. Moretti, P. Thevenard, D. Poker, *Thin Solid Films* 259 (1995) 113.
- [27] F. Mercier, C. Alliot, L. Bion, N. Thomat, P. Toulhoat, *J. Electron Spectrosc.* 150 (2006) 21.
- [28] I. Zareba-Grodz, R. Pazik, W. Tylus, W. Mielcarek, K. Hermanowicz, W. Strek, K. Maruszewski, *Opt. Mater.* 29 (2007) 1103.
- [29] C.R. Tewell, S.H. King, *Appl. Surf. Sci.* 253 (2006) 2597.
- [30] L. Armelao, S. Gross, G. Obeti, E. Tondello, *Surf. Coat. Technol.* 109 (2005) 218.
- [31] G. Speranza, L. Calliari, M. Ferrari, A. Chiasera, K. Trang Ngoc, A.M. Baranov, V.V. Slepstov, A.A. Nefedov, A.E. Varfolomeev, S.S. Fanchenko, *Appl. Surf. Sci.* 238 (2004) 117.
- [32] M.F. Al-Kuhaili, S.M.A. Durrani, *Thin Solid Films* 515 (2007) 2887.
- [33] Y.Y. Zhu, R. Xu, S. Chen, Z.B. Fang, F. Xue, Y.L. Fan, X.J. Yang, Z.M. Jiang, *Thin Solid Films* 508 (2006) 86.

- [34] A. Bouzidi, N. Benramdane, H. Tabet-Derraz, C. Mathieu, B. Khelifa, R. Desfeux, *Mater. Sci. Eng. B* 97 (2003) 5.
- [35] Y.B. Zheng, S.J. Wang, A.C.H. Huan, C.Y. Tan, L. Yan, C.K. Ong, *Appl. Phys. Lett.* 86 (2005) 112910.
- [36] M. Uno, A. Kosuga, M. Okui, K. Horisaka, H. Muta, K. Kurosaki, S. Yamanaka, *J. Alloys Compd.* 420 (2006) 291.
- [37] S. Chang, R. Doong, *J. Phys. Chem. B* 108 (2004) 18098.
- [38] A. Hartridge, M. Ghanashyam Krishna, A.K. Bhattacharya, *Thin Solid Films* 384 (2001) 254.
- [39] G. Ehrhart, M. Bouazaoui, B. Capoen, V. Ferreiro, R. Mahiou, O. Robbe, S. Turrell, *Opt. Mater.* 29 (2007) 1723.
- [40] F. Wang, X. Fan, D. Pi, Z. Wang, M. Wang, *J. Solid State Chem.* 178 (2005) 825.
- [41] Y. Tao, G. Zhao, X. Ju, X. Shao, W. Zhang, *Mater. Lett.* 28 (1996) 137.
- [42] W. Que, Y. Zhou, Y.L. Lam, K. Pita, Y.C. Chan, C.H. Kam, *Appl. Phys. A* 73 (2001) 209.
- [43] P. Salas, C. Angeles-Chavez, J.A. Montoya, E. De la Rosa, L.A. Diaz-Torres, H. Desirena, A. Martínez, M.A. Romero-Romo, J. Morales, *Opt. Mater.* 27 (2005) 1295.